biosensors

MDPI

Article

Aptamer-Based Graphene Field-Effect Transistor Biosensor for Cytokine Detection in Undiluted Physiological Media for Cervical Carcinoma Diagnosis

Ziran Wang [1,*], Wenting Dai [2], Zaiyu Zhang [1] and Haipeng Wang [1]

[1] Key Laboratory of High-Efficiency and Clean Mechanical Manufacture of MOE, School of Mechanical Engineering, Shandong University, Jinan 250100, China
[2] Department of Mechanical Engineering, Columbia University, New York, NY 10027, USA
* Correspondence: wangziran@sdu.edu.cn

Abstract: Personalized monitoring of disease biomarkers is of great interest in women's health. However, existing approaches typically involve invasive inspection or bulky equipment, making them challenging to implement at home. Hence, we present a general strategy for label-free and specific detection of disease biomarkers in physiological media using an aptamer-based biosensor. The biosensor is a graphene field-effect transistor that involves immobilizing the aptamer and a biomolecule-permeable polyethylene glycol (PEG) layer on the graphene surface. The aptamer is capable of specifically binding with the target biomarker, thus inducing a change in the sensing responses. The PEG layer can effectively reduce the nonspecific adsorption of nontarget molecules in the solution, and increase the effective Debye screening length in the region directly adjacent to the graphene. In this work, studies of a biosensor with modification of the aptamer and PEG show that cervical carcinoma biomarkers such as tumor necrosis factor-α and interleukin 6 can be sensitively and specifically detected in undiluted physiological media, with detection limits as low as 0.13 pM for TNF-a and 0.20 pM for IL-6. This work presents a significant method for the general application of the biosensor for disease diagnosis in women's health.

Keywords: graphene field-effect transistor; biosensor; cytokine; physiological media; cervical carcinoma

Received: 26 January 2025
Revised: 20 February 2025
Accepted: 21 February 2025
Published: 23 February 2025

Citation: Wang, Z.; Dai, W.; Zhang, Z.; Wang, H. Aptamer-Based Graphene Field-Effect Transistor Biosensor for Cytokine Detection in Undiluted Physiological Media for Cervical Carcinoma Diagnosis. *Biosensors* **2025**, *15*, 138. https://doi.org/10.3390/bios15030138

1. Introduction

Cervical carcinoma, which gives rise to severe complications involving multiple systems such as the reproductive, digestive, and lymphatic systems, is a highly pathogenic malignant tumor for women. Recent studies indicate that cervical carcinoma primarily exhibits clinical symptoms such as abdominal discomfort and bloating, similar to other gynecological conditions [1,2]. Although imaging studies are useful in detecting abnormalities, the nonspecific symptoms of cervical carcinoma frequently make early diagnosis challenging. Consequently, it is highly desirable to develop a device for diagnosing and predicting the severity of ovarian cancer, offering the essential reference for the population's self-diagnostics in daily life or aiding clinical diagnoses.

Physiological media (e.g., sweat and lavage fluid), containing numerous disease biomarkers, could potentially reflect the human body's deeper physiological state [3–5]. Cytokines such as tumor necrosis factor alpha (TNF-α) and interleukin-6 (IL-6) have been reported in subjects with many severe diseases, such as cervical carcinoma and ovarian cancer [6,7]. Particularly, research shows that an abnormal concentration of cytokines in

physiological media is critical in the diagnosis of cervical carcinoma or in predicting its severity [8,9]. Hence, developing biosensors that enable rapid and sensitive detection of cytokines in physiological media is of great significance for the diagnosing and monitoring of cervical carcinoma patients' conditions [10–12].

Recently, aptamer-based biosensors have been developed to detect disease biomarkers. Such sensors involve using antibodies or aptamers as specific probes to recognize target molecules [13,14]. In particular, aptamer-based field-effect transistors configure from semiconductor materials [15], carbon nanotubes [16] and graphene [17] have received significant attention for biosensing applications. Among these materials, graphene is an ideal candidate as the conducting channel for biosensors, due to the unique characteristics such as high carrier mobility, low intrinsic noise and sensitive to its surface charge distribution [18–20]. Since the first investigation of biomarker detection using the graphene-based field-effect transistor (GFET) [21], such devices have demonstrated high sensitivity and specificity in label-free detection of various analytes, including ions, enzymes, small molecules, DNA, and proteins [22–24].

Biosensor development has been aimed at facilitating the creation of devices in the sensitive monitoring of biomarkers within authentic physiological media [25–27]. However, physiological media contains numerous biomolecules beyond the intended targets, encompassing metabolites (e.g., glucose and lactate), simple ions (e.g., Na^+ and Ca^{2+}) and cells. These nontarget molecules in such solutions tend to adsorb onto the graphene surface, introducing interference with biomarker detection. This interference reduces sensor sensitivity, making it challenging for the biosensor to effectively detect its targets in undiluted physiological media. Consequently, a necessity to investigate the capability of aptamer-based graphene biosensors arises, for sensitive detection of disease biomarkers in undiluted physiological media. To address nonspecific adsorption at graphene interfaces, reagents such as Nafion [28], Tween 20 [29], and, particularly, polyethylene glycol (PEG) [30] are utilized. PEG, recognized for its biocompatibility, enhances the Debye screening length in high ionic strength media, also offering its reliable attachment to device surfaces to reduce nonspecific interactions in physiological media [31,32]. However, these biosensors require FET analysis in PBS (phosphate-buffered saline) or diluted media, limiting their suitability for direct, in situ disease diagnostics under real clinical conditions. Consequently, there arises a need to investigate the capability of aptamer-based graphene biosensors for sensitive monitoring of disease biomarkers in physiological media.

This paper achieves a direct and sensitive measurement of cytokines in undiluted physiological media using an aptamer-based GFET biosensor modified with a biomolecule-permeable polyethylene glycol (PEG) isolation layer. The biosensor is configured from a graphene conducting channel covered with a PEG, and is functionalized with the aptamer specific to the biomarker to be measured (Figure 1a). Binding of the aptamer probe with the biomarker induces a change in the electric conductivity of the graphene, which is measured via the current between drain/source electrodes in solution environments to determine the cytokine concentration (Figure 1b). The modification of graphene with PEG isolation layer is investigated, which offers the effective elimination of interferences from the nonspecific adsorption and enhances the sensitivity of the biosensor (Figure 2a). Experimental results demonstrate that the biosensor enables sensitive detection of cytokines (e.g., TNF-α and IL-6), representative cervical carcinoma severity biomarkers, in undiluted physiological media (e.g., artificial sweat and lavage fluid) with limits of detection (LOD) as low as 0.13 pM for TNF-a and 0.20 pM for IL-6. With these capabilities, the aptamer-based GFET biosensor can be potentially used in daily noninvasive and rapid cervical carcinoma detection in human biofluids.

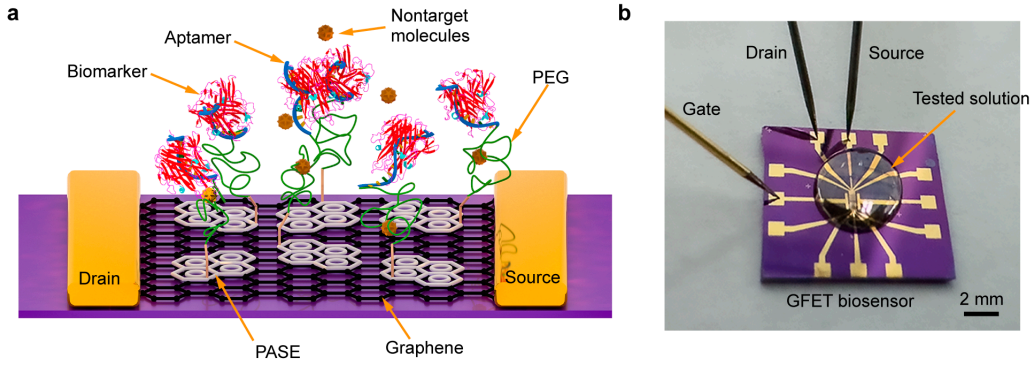

Figure 1. Aptamer-based GFET biosensor. (**a**) Schematic of the biosensor with the modification of PEG and aptamer used in this work. (**b**) Photograph of the biosensor for biomarker detection.

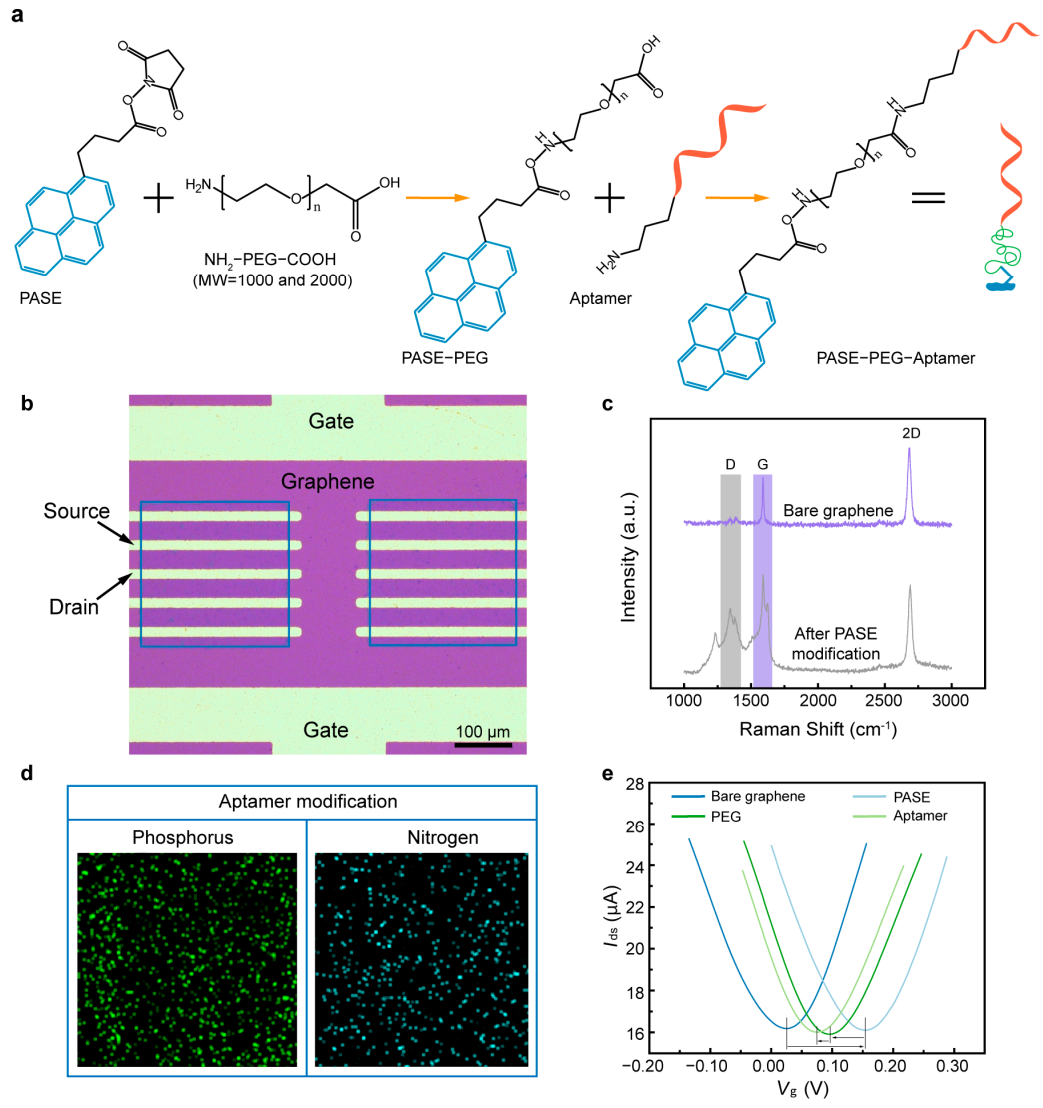

Figure 2. Surface modification of the GFET biosensor. (**a**) Schematic of the biosensor modification processes. (**b**) Microscope image of the biosensor with graphene conducting channel and electrodes. (**c**) Raman spectra of the graphene before and after PASE modification. (**d**) EDS of the biosensor after aptamer modification. (**e**) Transfer characteristic curves of functionalization processes of the graphene conducting channel.

2. Materials and Methods

2.1. Materials

Chemical vapor deposition (CVD) graphene was purchased from Nanjing Muke Nanotechnology (Nanjing, China). 1-Pyrenebutyric acid N-hydroxysuccinimide ester (PASE), ethanolamine, 1-ethyl-3-(3-dimethylaminepropyl) carbodiimide hydrochloride (EDC•HCl), N-hydroxysulfosuccinimide (NHS) and human Interleukin-002 (IL-002) were ordered from Sigma-Aldrich. Various lengths of PEG polymers were purchased from Creative PEGWorks. Artificial sweat was purchased from Walgreens. TNF-α, IL-6 and IFN-gamma (IFN-γ) were purchased from R&D Systems. Aptamer (5′-NH_2-TGG TGG ATG GCG CAG TCG GCG ACA A-3′) for TNF-α detection and 5′-NH_2-GGT GGC AGG AGG ACT ATT TAT TTG CTT TTC T-3′ for IL-6 detection were synthesized and purified by Sangong Biotech (Shanghai, China).

2.2. Aptamer-Based Biosensor Design and Fabrication

The design and fabrication of the GFET biosensor is described in detail in the previous study [17]. Briefly, drain–source and on-chip gate electrodes were patterned onto SiO_2 wafers using Ti/Au deposition (2 nm/38 nm), and then a monolayer graphene grown by chemical vapor deposition was transferred onto the drain–source electrode as a conducting channel. A microscope image of integrated GFET biosensor with graphene-based conducting channel (50 μm) is shown in Figure 2b. During operation, a sweeping gating voltage and consistent drain–source voltage were applied to the conducting channel, thereby generating drain–source current in the graphene. The change in the drain–source current arising from the aptamer–biomarker interaction is measured to determine the biomarker concentration.

2.3. Surface Modification and Characterization

The modification processes were carried out to enable cytokine detection by PEG and aptamer functionalization. 1-pyrenebutanoic acid succinimidyl ester (PASE) was first modified on the graphene through π-π stacking, which was used to immobilize NH_2-PEG-COOH. Then, ethanolamine was used to quench the unreacted PASE. The mixture solution of EDC•HCl and NHS was used to activate the carboxylic group at the end of the PEG, enabling a condensation reaction of amino on the aptamer and activated carboxyl groups on the PEG. (Figure 2a) Finally, ethanolamine was used to occupy the unreacted PEG. The functionalization of graphene with PASE was verified using Raman spectra under 532 nm laser excitation (Figure 2c). The split of the G band and the remarkable D band were observed after PASE modification, confirming the coupling of graphene and pyrene groups on PASE. The successful modification of the aptamer was verified using energy dispersive spectroscopy (EDS). Phosphorus and nitrogen were observed to exist in significant amounts on the graphene surface; these are the unique constituent elements of the aptamer (Figure 2d). Further, the electrical signal of each modification process was investigated by analyzing the measured transfer characteristic curves (Figure 2e). The Dirac point (V_{Dirac}) was observed to increase from 24 to 153 mV after PASE modification, and then decrease by 57 mV after NH_2-PEG-COOH immobilization. Upon covalent coupling of the aptamer, V_{Dirac} decreased from 96 to 76 mV, suggesting that the modification induced n-type doping in the graphene. These results illustrate that the biosensor was successfully functionalized using PEG and aptamer.

3. Results

3.1. Detection of TNF-α in PBS

The detection capability of the biosensor was first investigated in PBS using the biosensor modified with 1000 Da and 2000 Da PEG. TNF-α, a cytokine produced by white

blood cells, plays a key role in regulating immune and inflammatory responses [33–35]. Studies indicate that abnormal concentrations of TNF-α suggest its critical role in the molecular pathogenesis of cervical carcinoma and offer a potential biomarker for the early diagnosis and therapy of the disease [36–38]. The sensing mechanism relies on the structural transformation of the aptamer upon binding with proteins (Figure 3). This guanine-rich oligonucleotide sequence can adopt a compact and stable G-quadruplex structure, formed by two guanine tetrads originating from its loop region. Hence, TNF-α protein (isoelectric points is arounds 6.0), negatively charged in 1 × PBS, closely approached the graphene through binding with the aptamer. This interaction altered the conductivity of the graphene, thereby inducing n-type doping in graphene and resulting in a negative shift in the transfer characteristic curve. As shown in Figure 4a,b, the transfer characteristic curves continuously shifted towards the negative side of the X-axis as the concentration of TNF-α increased from 0.008 to 125 nM. For the biosensor modified with 1000 Da PEG, ΔV_{Dirac} shifted from −58 to −97 mV, and the value of ΔV_{Dirac} decreased from −1 to −31 mV for the biosensor modified with 2000 Da PEG.

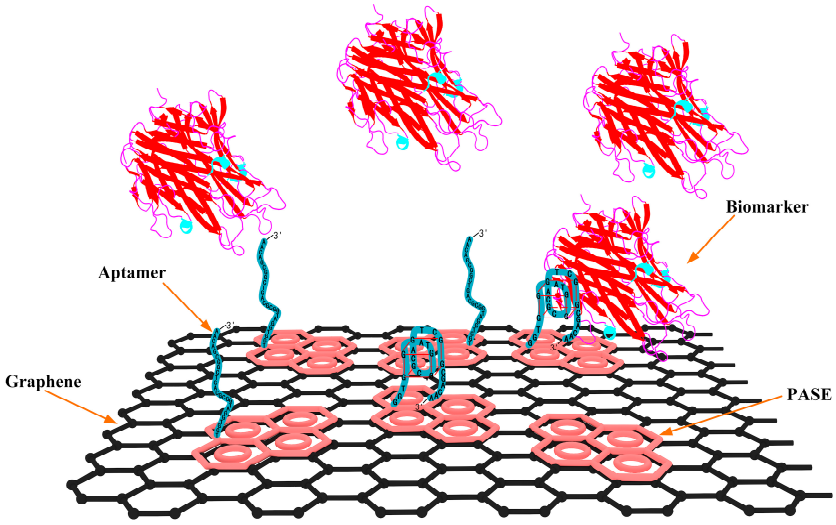

Figure 3. Schematic showing the conformation change in the aptamer upon binding with proteins.

To investigate the binding affinity between the aptamer and the TNF-α protein, a Hill–Langmuir binary binding model was applied to the characterized dissociation constant K_D of the biosensor. The non-linear approximation of the fitted curve was calculated based on the Hill–Langmuir equation, which is widely used in biochemical characterization (Figure 4c inset) [39,40].

$$\Delta V_{Dirac} = \frac{\Delta V_{Dirac,max} C_{TNF\text{-}\alpha}}{K_D + C_{TNF\text{-}\alpha}} \quad (1)$$

where $\Delta V_{Dirac,max}$ is the saturated shift of V_{Dirac}, and $C_{TNF\text{-}\alpha}$ is the TNF-α concentration. K_D represents the affinity between the aptamer and the TNF-α protein; a lower K_D value corresponds to a higher binding affinity. The impact of device variations on responses was mitigated by normalizing the Dirac point shift, defined as $\Delta V_{Dirac}/\Delta V_{Dirac,max}$, which was plotted as a function of TNF-α concentration for the biosensor with PEG modification (Figure 4c) or without PEG modification (Figure S1). From fitted curves, K_D values were calculated as 1.52 ± 0.35 nM, 1.21 ± 0.44 nM, and 2.82 ± 0.19 nM for biosensors modified with 1000 and 2000 Da PEG, and those without PEG modification in PBS, respectively. The increased value in K_D for the biosensor without PEG modification suggests that the presence of PEG on the surface contributes to the sensing response due to the increased Debye length [31,32]. Thus, PEG-modified biosensors exhibit a highly sensitive response

in biomarker detection, with a lower LOD and response time than seen in most existing methods (Table 1).

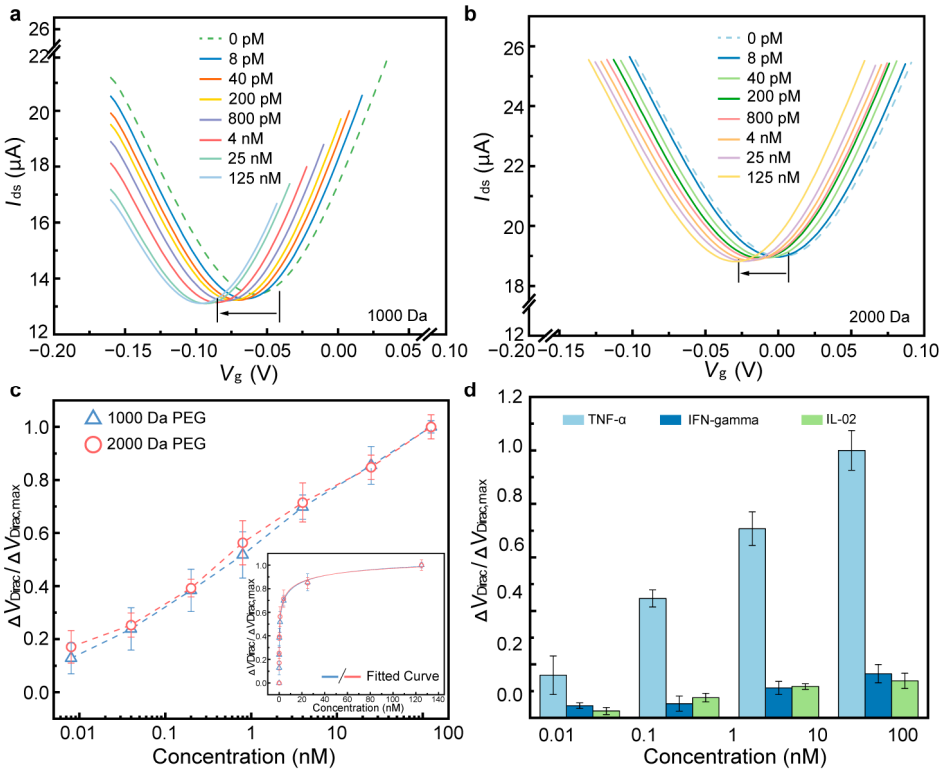

Figure 4. Biomarker detection in PBS. Transfer characteristic curves of the sensing response to different TNF-α concentrations in PBS using the biosensor modified with 1000 (**a**) and 2000 Da PEG (**b**). (**c**) $\Delta V_{Dirac}/\Delta V_{Dirac,max}$ as a function of TNF-α concentrations in PBS. The inset shows the fitted curves of the sensing responses. (**d**) $\Delta V_{Dirac}/\Delta V_{Dirac,max}$ show the responses to different TNF-α concentrations and the control proteins (IFN-γ and IL-002) in PBS.

Table 1. Comparison of the PEG-modified biosensors with existing methods.

Methods	Materials	Test Time	Limit of Detection	Ref.
Biolayer interferometry-based	Antibody Aptamer	11.5 min	62.5 pM	[41]
Optical sensor	Aptamer	N/A	98.23 pM	[42]
Optical sensor	Aptamer	5 min	2.24 pM	[43]
Electrochemical aptasensor	Aptamer	30 min	315.48 pM	[44]
Microfluidic device	Aptamer	30 min	288.9 pM	[45]
Field-effect transistor	Aptamer	5 min	0.13 pM	This work

Before testing the target protein, it is crucial to validate the biosensor's specificity and ensure that the sensing signal is generated by targets rather than nontarget molecules. Therefore, control proteins, such as IFN-γ and IL-02, which belong to the same cytokine family as TNF-α, were selected. TNF-α and control proteins were prepared in PBS with concentrations of 0.01, 0.1, 1, 10, and 100 nM, respectively. As shown in Figure 4d, the sensing responses of control proteins were negligible compared with TNF-α. The value of $\Delta V_{Dirac}/\Delta V_{Dirac,max}$ for control proteins was more than six times lower than that for TNF-α, indicating that the biosensor exhibits high specificity for the target biomarker.

3.2. Detection of TNF-α in Undiluted Artificial Sweat

To further verify the detection capability of PEG-modified biosensors in the physiological media, we conducted biomarker detection in artificial sweat. The biosensor modified with 1000 Da PEG only offered the capability of biomarker detection in 10 × diluted artificial sweat (Figure 5a), and ΔV_{Dirac} decreased from −114 to −140 mV, which is highly consistent with that tested in PBS (Figure 4a). Based on the fitted curve, K_D was calculated to be 1.39 ± 0.12 nM (Figure 5c), differing from the value seen in PBS by 8.6%, which suggested that the detection performance of the biosensor maintains high consistency with the corresponding value tested in PBS. However, the biosensor modified with 1000 Da PEG exhibits a minimal response to TNF-α concentrations below 25 nM in undiluted artificial sweat (Figure 5d), due to it not suppressing nonspecific adsorption. Moreover, the biosensor modified with 2000 Da PEG was tested in the measurement of TNF-α in undiluted artificial sweat (Figure 5b). The shift of ΔV_{Dirac} was 30 mV, the deviation of which, from the maximum ΔV_{Dirac} in PBS (32 mV), was less than 6.3%. K_D was estimated to be 1.24 ± 0.39 nM (Figure 5d), differing from the value found in the PBS test (1.21 ± 0.44 nM) by only 2.5% or less. In addition, experiments on biosensors without PEG modification were performed in undiluted artificial sweat (Figure S2). GFET shows the negligible sensing response compared with the biosensor modified with 2000 Da PEG, suggesting that PEG modification successfully suppresses nonspecific adsorption and enables biomarker detection in undiluted physiological media.

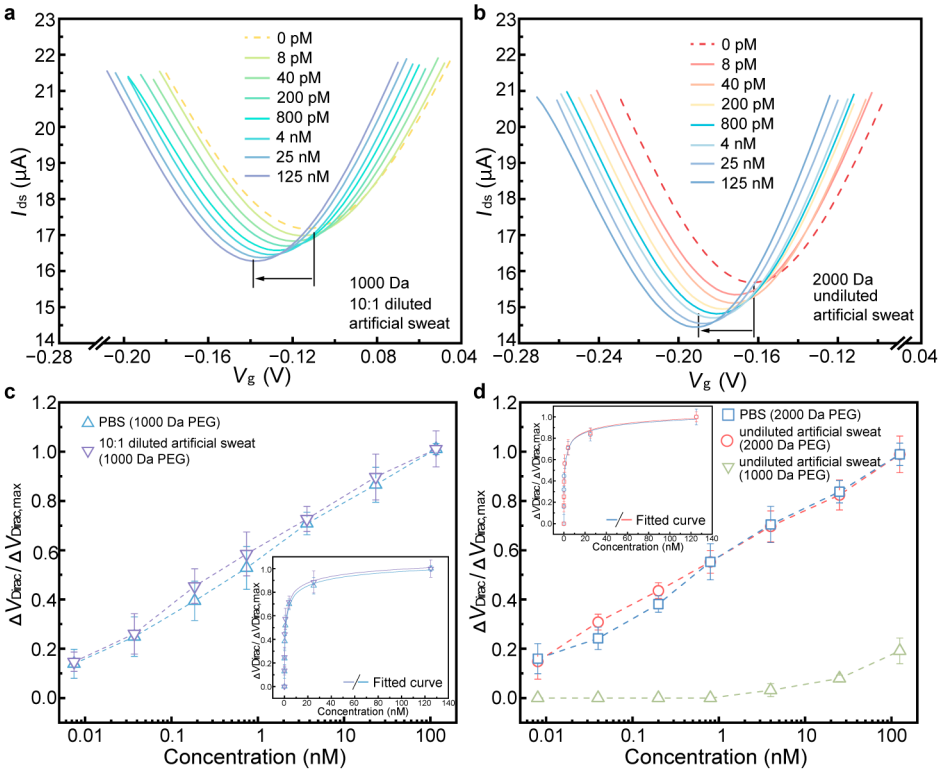

Figure 5. Biomarker detection in artificial sweat. Transfer characteristic curves of sensing responses to different TNF-α concentrations modified with 1000 Da PEG in 10× times diluted artificial sweat (**a**) and modified with 2000 Da PEG in undiluted artificial sweat (**b**). (**c**) $\Delta V_{Dirac}/\Delta V_{Dirac,max}$ as a function of TNF-α concentrations using the biosensor modified with 1000 and 2000 Da PEG in 10× times diluted artificial sweat (**c**) and undiluted artificial sweat (**d**), respectively. The inset shows fitted curves of sensing responses.

The function of larger molecule weights in PEG was also investigated. The value of ΔV_{Dirac} changed from −46 to −77 mV for the 5000 Da PEG modified biosensor, whose

deviation from the maximum ΔV_{Dirac} for 2000 Da PEG was less than 3.3% (Figure S3). Based on the fitted curve, K_D was estimated to be 1.19 ± 0.23 nM, differing from the value of the 2000 Da PEG-modified biosensor by 4.0% (Figure S2). These results suggest that the 2000 Da PEG would be enough to occupy the vacant area of the graphene surface, thereby enabling a consistent response with the biosensor modified with 5000 or even larger Da PEG. The results above showed that the GFET biosensor maintains high consistency and sensitivity for biomarker detection in undiluted physiological media. This highly desirable behavior for the biosensor could be explained by attributes of the PEG polymer. PEG polymers enable a substantial decrease in the dielectric constant of aqueous solutions, and thus serve to increase the effective Debye screening length for high-ionic-strength solutions [31,32]. Also, PEG formed a permeable layer on the graphene surface, which minimizes nonspecific binding in physiological media by preventing nontarget molecules from attaching to the graphene surface.

3.3. Detection of IL-6 in Undiluted Lavage Fluid

Perfusion medium refers to the covering fluid collected after tissue lavage, which contains various biotargets such as tumor cells, cytokines, and microenvironment components. Detection of such media (e.g., through biochemical testing and immunoassays) offers significant value for the diagnosis, observation, and prognosis of cervical carcinoma [46–48]. Particularly, IL-6 (with isoelectric points around 5.0), a representative cytokine, has the capacity to indicate the progression and clinical characteristics of cervical carcinoma [49,50]. Monitoring of IL-6 in PBS was first investigated using the biosensor modified with 1000 and 2000 Da PEG, respectively (Figure 6a and Figure 6d). As the IL-6 concentration increased from 0.1 to 1 nM, the transfer characteristic curves continuously shift towards the negative side of X axis, and the maximum $\Delta V_{Dirac,max}$ shifts measured were, respectively, 27 (1000 Da PEG modification) and 33 mV (2000 Da PEG modification). Based on the fitted curve, K_D was calculated to be 84 ± 23 and 188 ± 52 pM in PBS (Figure 6c and Figure 6f), respectively, which shows improvements over the values reported in the previous literature [51,52].

The biosensor was next modified to detect IL-6 in undiluted lavage fluid. For the biosensor modified with 1000 Da PEG (Figure 6b), we observed that the sensing response was shifted by 20 mV, varying from the maximum shift tested in PBS by about 25%. K_D was calculated to be 570 ± 96 pM, showing a significant difference from the value in PBS (Figure 6c). These results also illustrate that the biosensor modified with 1000 PEG was difficult to completely suppress in terms of nonspecific adsorption, thereby reducing the sensing response in undiluted physiological media. The response of the biosensor modified with 2000 Da PEG holds high consistency with that tested in PBS (Figure 6e). ΔV_{Dirac} was shifted by 29 mV, with a variation of less than 12%. The dissociation constant K_D was estimated to be 194 ± 23 pM in undiluted lavage fluid (Figure 6f), which deviated by less than 3.2% from the K_D in PBS. These results suggest that the biosensor modified with PEG was able to greatly reduce nonspecific adsorption on the graphene surface. Additionally, it illustrates that the molecular length of the PEG plays a significant role in the sensing response, as the biosensor modified with 1000 Da PEG showed obvious signal attenuation in undiluted lavage fluid compared with 2000 Da PEG modification.

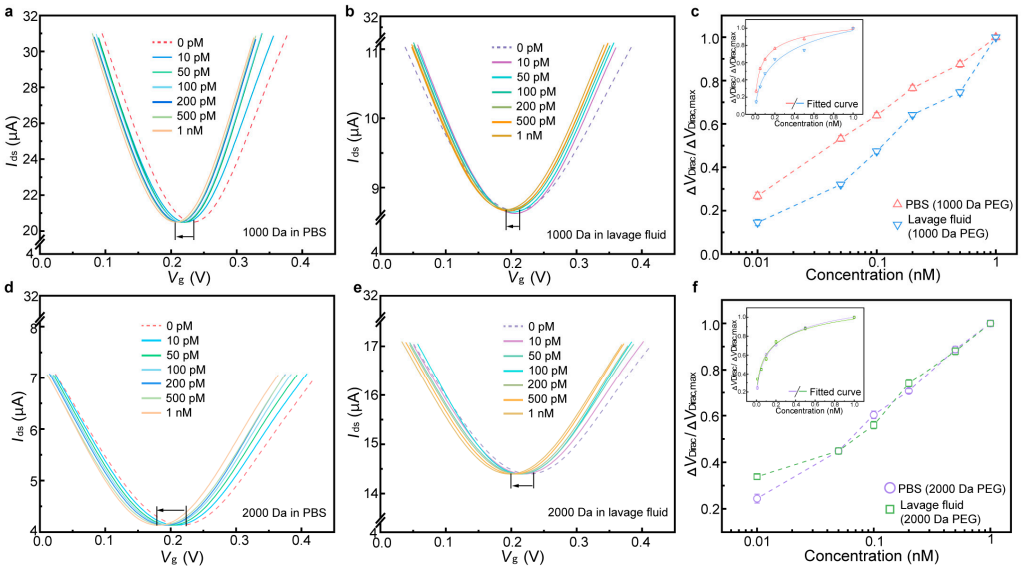

Figure 6. Sensing response of the biosensor to the IL-6 biomarker. Transfer characteristic curves of the biosensor modified with 1000 Da PEG in response to different IL-6 concentrations in PBS (**a**) and undiluted perfusion media (**b**). (**c**) $\Delta V_{Dirac}/\Delta V_{Dirac,max}$ as a function of IL-6 concentrations in PBS and undiluted perfusion media (1000 Da PEG). The inset shows fitted curves of sensing responses. (**d**) Transfer characteristic curves of the biosensor modified with 2000 Da PEG in response to different IL-6 concentrations in PBS (**d**) and undiluted perfusion media (**e**). (**f**) $\Delta V_{Dirac}/\Delta V_{Dirac,max}$ as a function of IL-6 concentrations in PBS and undiluted perfusion media (2000 Da PEG). The inset shows fitted curves of sensing responses.

4. Discussion

The results above, which show the PEG-modified biosensor's success or failure in detecting biomarkers in undiluted physiological media, indicate that PEG length (molecular weight) offers a significant impact on biomarker detection rates in the high-ionic-strength solution. These highly desirable biosensor behaviors could mainly be explained as being effects of the suppression of nonspecific adsorption by the PEG polymer. For example, the biosensor modified with 1000/2000 Da PEG maintains a consistent sensing response in high-ionic solution (1 × PBS) (Figure 4). However, the biosensor modified with 1000 Da PEG shows a negligible sensing response for TNF-α concentrations below 25 nM in undiluted artificial sweat, and its sensing response declines more than 20% for IL-6 in undiluted lavage fluid (Figures 5d and 6c). These results illustrate that while Debye length may contribute to sensor response, its role in enabling measurement in physiological media may be secondary compared its role in the suppression of nonspecific adsorption. Longer PEG polymers cover more sites on the graphene surface, thereby enhancing their ability to prevent nonspecific binding. Consequently, the biosensor exhibits heightened sensitivity and specificity in physiological media, suggesting that optimal PEG modification could enable monitoring of various biomarkers in physiological media for point-of-care applications.

5. Conclusions

In summary, we demonstrated a general strategy for label-free, sensitive, and specific detection of biomarkers in high-ionic-strength physiological media using a graphene-based field-effect transistor biosensor modified with PEG. The aptamer specifically binds with the biomarker, and induced a change in the carrier concentration of the graphene, which was measured to determine the biomarker concentration. A porous and biomolecule-permeable PEG layer formed on the graphene surface reduced the nonspecific adsorption in physiological media (e.g., undiluted artificial sweat and lavage fluid). The biosensor thus

possesses highly sensitive and specific sensing responses to the biomarker in undiluted artificial sweat. In addition, the effect of PEG length on biomarker detection was studied. From the comparison of results, we believe that PEG length is one of the major factors that affects the biosensor's sensing capability in physiological media. In experiments, the biosensor modified with the aptamer and different lengths of PEG was capable of consistently and sensitively detecting the TNF-α protein in undiluted physiological media, achieving a repeatable LOD as low as 0.13 pM for TNF-a and 0.20 pM for IL-6. These results demonstrate that this strategy is a critical step toward the general application of the graphene-based biosensor in the monitoring of disease biomarkers.

Supplementary Materials: The following supporting information can be downloaded at: https://www.mdpi.com/article/10.3390/bios15030138/s1, Figure S1: $\Delta V_{Dirac}/\Delta V_{Dirac,max}$ as a function of TNF-α concentrations using the biosensor modified without/with 1000 Da and 2000 Da PEG in 1 × PBS; Figure S2: $\Delta V_{Dirac}/\Delta V_{Dirac,max}$ as a function of TNF-α concentrations using the biosensor modified without/with 1000 Da, 2000 Da and 5000 Da PEG in undiluted artificial sweat. Figure S3: Transfer characteristic curves of the sensing response in undiluted artificial sweat using the biosensor modified with 5000 Da PEG.

Author Contributions: Z.W. and W.D. contributed equally to this work. Z.W. and W.D. designed and performed testing experiments, measured graphene transistor devices, and prepared the original manuscript. Z.Z. and H.W. designed and fabricated transistor devices, and participated in data analysis. Z.W. supervised the project, revised the manuscript, and acquired funding. All authors have read and agreed to the published version of the manuscript.

Funding: This work was supported by the National Natural Science Foundation of China (Grant No. 52305606), Taishan Scholars Project of Shandong Province (Grant No. tsqn202306028), Shandong Provincial Natural Science Foundation (Grant No. ZR2023QE187), Natural Science Foundation of Jiangsu Province (Grant No. BK20230254), and the Qilu Young Scholars Program of Shandong University, State Key Laboratory of Robotics and System (HIT) (Grant No. SKLRS-2023-KF-03).

Data Availability Statement: All data are contained within the article.

Conflicts of Interest: The authors declare no conflicts of interest.

Abbreviations

The following abbreviations are used in this manuscript:

PEG	Polyethylene Glycol
GFET	Graphene-based Field-Effect Transistor
TNF-α	Tumor Necrosis Factor Alpha
IL-6	Interleukin-6
PASE	1-Pyrenebutyric Acid N-hydroxysuccinimide Ester
EDC•HCl	1-Ethyl-3-(3-dimethylaminepropyl) Carbodiimide Hydrochloride
NHS	N-Hydroxysulfosuccinimide
PBS	Phosphate-Buffered Saline

References

1. Volkova, L.V.; Pashov, A.I.; Omelchuk, N.N. Cervical carcinoma: Oncobiology and biomarkers. *Int. J. Mol. Sci.* **2021**, *22*, 12571. [CrossRef] [PubMed]
2. Chu, D.; Liu, T.; Yao, Y. Implications of viral infections and oncogenesis in uterine cervical carcinoma etiology and pathogenesis. *Front. Microbiol.* **2023**, *14*, 1194431. [CrossRef]
3. Emaminejad, S.; Gao, W.; Wu, E.; Davies, Z.A.; Nyein, H.Y.Y.; Challa, S.; Ryan, S.P.; Fahad, H.M.; Chen, K.; Shahpar, Z.; et al. Autonomous sweat extraction and analysis applied to cystic fibrosis and glucose monitoring using a fully integrated wearable platform. *Proc. Natl. Acad. Sci. USA* **2017**, *114*, 4625–4630. [CrossRef] [PubMed]

4. Gao, W.; Emaminejad, S.; Nyein, H.Y.Y.; Challa, S.; Chen, K.; Peck, A.; Fahad, H.M.; Ota, H.; Shiraki, H.; Kiriya, D.; et al. Fully integrated wearable sensor arrays for multiplexed in situ perspiration analysis. *Nature* **2016**, *529*, 509–514. [CrossRef] [PubMed]
5. Filipiak, M.S.; Rother, M.; Andoy, N.M.; Knudsen, A.C.; Grimm, S.; Bachran, C.; Swee, L.K.; Zaumseil, J.; Tarasov, A. Highly sensitive, selective and label-free protein detection in physiological solutions using carbon nanotube transistors with nanobody receptors. *Sens. Actuators B Chem.* **2018**, *255*, 1507–1516. [CrossRef]
6. Lupi, L.A.; Cucielo, M.S.; Silveira, H.S.; Gaiotte, L.B.; Cesário, R.C.; Seiva, F.R.F.; Chuffa, L.G.d.A. The role of Toll-like receptor 4 signaling pathway in ovarian, cervical, and endometrial cancers. *Life Sci.* **2020**, *247*, 117435. [CrossRef]
7. Manasa, G.; Mascarenhas, R.J.; Shetti, N.P.; Malode, S.J.; Aminabhavi, T.M. Biomarkers for early diagnosis of ovarian carcinoma. *ACS Biomater. Sci. Eng.* **2022**, *8*, 2726–2746. [CrossRef]
8. Kartikasari, A.E.; Huertas, C.S.; Mitchell, A.; Plebanski, M. Tumor-induced inflammatory cytokines and the emerging diagnostic devices for cancer detection and prognosis. *Front. Oncol.* **2021**, *11*, 692142. [CrossRef]
9. Pahne-Zeppenfeld, J.; Schröer, N.; Walch-Rückheim, B.; Oldak, M.; Gorter, A.; Hegde, S.; Smola, S. Cervical cancer cell-derived interleukin-6 impairs CCR7-dependent migration of MMP-9-expressing dendritic cells. *Int. J. Cancer* **2014**, *134*, 2061–2073. [CrossRef]
10. Mahmoodi, P.; Rezayi, M.; Rasouli, E.; Avan, A.; Gholami, M.; Mobarhan, M.G.; Karimi, E.; Alias, Y. Early-stage cervical cancer diagnosis based on an ultra-sensitive electrochemical DNA nanobiosensor for HPV-18 detection in real samples. *J. Nanobiotechnology* **2020**, *18*, 1–12. [CrossRef] [PubMed]
11. Kim, J.; Campbell, A.S.; De Ávila, B.E.-F.; Wang, J. Wearable biosensors for healthcare monitoring. *Nat. Biotechnol.* **2019**, *37*, 389–406. [CrossRef]
12. Bandodkar, A.J.; Jeang, W.J.; Ghaffari, R.; Rogers, J.A. Wearable sensors for biochemical sweat analysis. *Annu. Rev. Anal. Chem.* **2019**, *12*, 1–22. [CrossRef]
13. Kim, Y.S.; Raston NH, A.; Gu, M.B. Aptamer-based nanobiosensors. *Biosens. Bioelectron.* **2016**, *76*, 2–19.
14. Rajesh; Gao, Z.; Vishnubhotla, R.; Ducos, P.; Serrano, M.D.; Ping, J.; Robinson, M.K.; Johnson, A.T.C. Genetically engineered antibody functionalized platinum nanoparticles modified CVD-graphene nanohybrid transistor for the detection of breast cancer biomarker, HER3. *Adv. Mater. Interfaces* **2016**, *3*, 1600124. [CrossRef]
15. Nakatsuka, N.; Yang, K.A.; Abendroth, J.M.; Cheung, K.M.; Xu, X.; Yang, H.; Zhao, C.; Zhu, B.; Rim, Y.S.; Yang, Y.; et al. Aptamer–field-effect transistors overcome Debye length limitations for small-molecule sensing. *Science* **2018**, *362*, 319–324. [CrossRef]
16. Kara, P.; de la Escosura-Muñiz, A.; Maltez-da Costa, M.; Guix, M.; Ozsoz, M.; Merkoçi, A. Aptamers based electrochemical biosensor for protein detection using carbon nanotubes platforms. *Biosens. Bioelectron.* **2010**, *26*, 1715–1718. [CrossRef] [PubMed]
17. Wang, Z.; Hao, Z.; Yu, S.; De Moraes, C.G.; Suh, L.H.; Zhao, X.; Lin, Q. An Ultraflexible and Stretchable Aptameric Graphene Nanosensor for Biomarker Detection and Monitoring. *Adv. Funct. Mater.* **2019**, *29*, 1905202. [CrossRef] [PubMed]
18. Kim, B.J.; Jang, H.; Lee, S.K.; Hong, B.H.; Ahn, J.H.; Cho, J.H. High-Performance Flexible Graphene Field Effect Transistors with Ion Gel Gate Dielectrics. *Nano Lett.* **2010**, *10*, 3464–3466. [CrossRef] [PubMed]
19. Geim, A.K.; Novoselov, K.S. The rise of graphene. *Nat. Mater.* **2009**, *6*, 11–19.
20. Choi, D.; Choi, M.; Choi, W.M.; Shin, H.; Park, H.; Seo, J.; Park, J.; Yoon, S.; Chae, S.J.; Lee, Y.H.; et al. Fully Rollable Transparent Nanogenerators Based on Graphene Electrodes. *Adv. Mater.* **2010**, *22*, 2187–2192. [CrossRef] [PubMed]
21. Ohno, Y.; Maehashi, K.; Matsumoto, K. Label-Free Biosensors Based on Aptamer-Modified Graphene Field-Effect Transistors. *J. Am. Chem. Soc.* **2010**, *132*, 18012–18013. [CrossRef] [PubMed]
22. Shao, Y.; Wang, J.; Wu, H.; Liu, J.; Aksay, I.A.; Lin, Y. Graphene Based Electrochemical Sensors and Biosensors: A Review. *Electroanalysis* **2010**, *22*, 1027–1036. [CrossRef]
23. Song, Y.; Luo, Y.; Zhu, C.; Li, H.; Du, D.; Lin, Y. Recent Advances in Electrochemical Biosensors based on Graphene Two-Dimensional Nanomaterials. *Biosens. Bioelectron.* **2015**, *76*, 195. [CrossRef]
24. Bollella, P.; Fusco, G.; Tortolini, C.; Sanzò, G.; Favero, G.; Gorton, L.; Antiochia, R. Beyond graphene: Electrochemical sensors and biosensors for biomarkers detection. *Biosens. Bioelectron.* **2016**, *89 Pt 1*, 152–166. [CrossRef] [PubMed]
25. Andoy, N.M.; Filipiak, M.S.; Vetter, D.; Gutierrez-Sanz, O.; Tarasov, A. Graphene-Based Electronic Immunosensor with Femtomolar Detection Limit in Whole Serum. *Adv. Mater. Technol.* **2018**, *3*, 12. [CrossRef]
26. Kim, J.; Sempionatto, J.R.; Imani, S.; Hartel, M.C.; Barfidokht, A.; Tang, G.; Campbell, A.S.; Mercier, P.P.; Wang, J. Simultaneous monitoring of sweat and interstitial fluid using a single wearable biosensor platform. *Adv. Sci.* **2018**, *5*, 1800880. [CrossRef] [PubMed]
27. Brothers, M.C.; DeBrosse, M.; Grigsby, C.C.; Naik, R.R.; Hussain, S.M.; Heikenfeld, J.; Kim, S.S. Achievements and challenges for real-time sensing of analytes in sweat within wearable platforms. *Acc. Chem. Res.* **2019**, *52*, 297–306. [CrossRef] [PubMed]
28. Wee, K.W.; Kang, G.Y.; Park, J.; Kang, J.Y.; Yoon, D.S.; Park, J.H.; Kim, T.S. Novel electrical detection of label-free disease marker proteins using piezoresistive self-sensing micro-cantilevers. *Biosens. Bioelectron.* **2005**, *20*, 1932–1938. [CrossRef] [PubMed]

29. Chang, H.-K.; Ishikawa, F.N.; Zhang, R.; Datar, R.; Cote, R.J.; Thompson, M.E.; Zhou, C. Rapid, label-free, electrical whole blood bioassay based on nanobiosensor systems. *ACS Nano* **2011**, *5*, 9883–9891. [CrossRef] [PubMed]
30. Sun, C.; Miao, J.; Yan, J.; Yang, K.; Mao, C.; Ju, J.; Shen, J. Applications of antibiofouling PEG-coating in electrochemical biosensors for determination of glucose in whole blood. *Electrochim. Acta* **2013**, *89*, 549–554. [CrossRef]
31. Kohonen, M.M.; Karaman, M.E.; Pashley, R.M. Debye length in multivalent electrolyte solutions. *Langmuir* **2000**, *16*, 5749–5753. [CrossRef]
32. Arnold, K.; Herrmann, A.; Pratsch, L.; Gawrisch, K. The dielectric properties of aqueous solutions of poly (ethylene glycol) and their influence on membrane structure. *Biochim. Biophys. Acta (BBA)-Biomembr.* **1985**, *815*, 515–518. [CrossRef]
33. Balkwill, F. TNF-α in promotion and progression of cancer. *Cancer Metastasis Rev.* **2006**, *25*, 409–416. [CrossRef] [PubMed]
34. Popa, C.; Netea, M.G.; Van Riel, P.L.; Van Der Meer, J.W.; Stalenhoef, A.F. The role of TNF-α in chronic inflammatory conditions, intermediary metabolism, and cardiovascular risk. *J. Lipid Res.* **2007**, *48*, 751–762. [CrossRef] [PubMed]
35. Zganiacz, A.; Santosuosso, M.; Wang, J.; Yang, T.; Chen, L.; Anzulovic, M.; Alexander, S.; Gicquel, B.; Wan, Y.; Bramson, J.; et al. TNF-α is a critical negative regulator of type 1 immune activation during intracellular bacterial infection. *J. Clin. Investig.* **2004**, *113*, 401–413. [CrossRef]
36. Zijlmans, H.J.; Fleuren, G.J.; Baelde, H.J.; Eilers, P.H.; Kenter, G.G.; Gorter, A. Role of tumor-derived proinflammatory cytokines GM-CSF, TNF-α, and IL-12 in the migration and differentiation of antigen-presenting cells in cervical carcinoma. *Cancer Interdiscip. Int. J. Am. Cancer Soc.* **2007**, *109*, 556–565. [CrossRef] [PubMed]
37. E Lages, E.L.; Belo, A.V.; Andrade, S.P.; Rocha, M.Â.; de Freitas, G.F.; Lamaita, R.M.; Traiman, P.; Silva-Filho, A.L. Analysis of systemic inflammatory response in the carcinogenic process of uterine cervical neoplasia. *Biomed. Pharmacother.* **2011**, *65*, 496–499. [CrossRef] [PubMed]
38. Ma, Y.; Zhang, X.; Yang, J.; Jin, Y.; Xu, Y.; Qiu, J. Comprehensive molecular analyses of a TNF family-based gene signature as a potentially novel prognostic biomarker for cervical cancer. *Front. Oncol.* **2022**, *12*, 854615. [CrossRef]
39. Wang, C.; Liu, R.; Zhang, W.; Wang, Y.; Xu, K.; Yue, Z.; Liu, G. Multichannel scan surface plasmon resonance biochip with stationary optics and baseline updating capability. *J. Biomed. Opt.* **2013**, *18*, 115002. [CrossRef]
40. Duan, X.; Li, Y.; Rajan, N.K.; Routenberg, D.A.; Modis, Y.; Reed, M.A. Quantification of the affinities and kinetics of protein interactions using silicon nanowire biosensors. *Nat. Nanotechnol.* **2012**, *7*, 401–407. [CrossRef]
41. Gao, S.; Cheng, Y.; Zhang, S.; Zheng, X.; Wu, J. A biolayer interferometry-based, aptamer–antibody receptor pair biosensor for real-time, sensitive, and specific detection of the disease biomarker TNF-α. *Chem. Eng. J.* **2022**, *433*, 133268. [CrossRef]
42. Ghosh, S.; Datta, D.; Chaudhry, S.; Dutta, M.; Stroscio, M.A. Rapid detection of tumor necrosis factor-alpha using quantum dot-based optical aptasensor. *IEEE Trans. Nanobioscience* **2018**, *17*, 417–423. [CrossRef] [PubMed]
43. Baydemir, G.; Bettazzi, F.; Palchetti, I.; Voccia, D. Strategies for the development of an electrochemical bioassay for TNF-alpha detection by using a non-immunoglobulin bioreceptor. *Talanta* **2016**, *151*, 141–147. [CrossRef] [PubMed]
44. Liu, Y.; Matharu, Z.; Rahimian, A.; Revzin, A. Detecting multiple cell-secreted cytokines from the same aptamer-functionalized electrode. *Biosens. Bioelectron.* **2015**, *64*, 43–50. [CrossRef] [PubMed]
45. Kwa, T.; Zhou, Q.; Gao, Y.; Rahimian, A.; Kwon, L.; Liu, Y.; Revzin, A. Reconfigurable microfluidics with integrated aptasensors for monitoring intercellular communication. *Lab A Chip* **2014**, *14*, 1695–1704. [CrossRef] [PubMed]
46. Van Raemdonck, G.A.; Tjalma, W.A.; Coen, E.P.; Depuydt, C.E.; Van Ostade, X.W. Identification of protein biomarkers for cervical cancer using human cervicovaginal fluid. *PLoS ONE* **2014**, *9*, e106488. [CrossRef]
47. Liu, J.; Sun, H.; Wang, X.; Yu, Q.; Li, S.; Yu, X.; Gong, W. Increased exosomal microRNA-21 and microRNA-146a levels in the cervicovaginal lavage specimens of patients with cervical cancer. *Int. J. Mol. Sci.* **2014**, *15*, 758–773. [CrossRef] [PubMed]
48. Cai, Y.; Zhai, J.; Wu, Y.; Chen, R.; Tian, X. The role of IL-2, IL-4, IL-10 and IFN-γ cytokines expression in the microenvironment of cervical intraepithelial neoplasia. *Adv. Reprod. Sci.* **2022**, *10*, 106–114. [CrossRef]
49. Unver, N.; Mcallister, F. IL-6 family cytokines: Key inflammatory mediators as biomarkers and potential therapeutic targets. *Cytokine Growth Factor Rev.* **2018**, *41*, 10–17. [CrossRef] [PubMed]
50. Vilotić, A.; Nacka-Aleksić, M.; Pirković, A.; Bojić-Trbojević, Ž.; Dekanski, D.; Krivokuća, M.J. IL-6 and IL-8: An overview of their roles in healthy and pathological pregnancies. *Int. J. Mol. Sci.* **2022**, *23*, 14574. [CrossRef] [PubMed]
51. Khan, N.I.; Song, E. Detection of an IL-6 biomarker using a GFET platform developed with a facile organic solvent-free aptamer immobilization approach. *Sensors* **2021**, *21*, 1335. [CrossRef]
52. Liu, L.S.; Wang, F.; Ge, Y.; Lo, P.K. Recent developments in aptasensors for diagnostic applications. *ACS Appl. Mater. Interfaces* **2020**, *13*, 9329–9358. [CrossRef] [PubMed]